energy&fuels

Article

pubs.acs.org/EF

Stability Assessment of Regenerated Hierarchical ZSM-48 Zeolite Designed by Post-Synthesis Treatment for Catalytic Cracking of Light Naphtha

Mohamed H. M. Ahmed,[†] Oki Muraza,[*,†] Shota Nakaoka,[‡] Anas K. Jamil,[†] Alvaro Mayoral,[§] Victor Sebastian,[∥,⊥] Zain H. Yamani,[†] and Takao Masuda[‡]

[†]Center of Excellence in Nanotechnology and Chemical Engineering Department, King Fahd University of Petroleum and Minerals, Dhahran 31261, Saudi Arabia

[‡]Division of Chemical Process Engineering, Faculty of Engineering, Hokkaido University, N13-W8, Kita-ku, Sapporo, Hokkaido 060-8628, Japan

[§]Advanced Microscopy Laboratory (LMA), Institute of Nanoscience of Aragon (INA) and [∥]Department of Chemical Engineering and Environmental Technology and Institute of Nanoscience of Aragon (INA), Universidad de Zaragoza, Mariano Esquillor, Building I+D, 50018 Zaragoza, Spain

[⊥]Biomedical Networking Research Center on Bioengineering, Biomaterials and Nanomedicine (CIBER-BBN), 28029 Madrid, Spain

ABSTRACT: Hierarchical ZSM-48, a one-dimensional pore system zeolite with the presence of mesopores, was obtained by post-synthesis alkaline and acid treatments. Hierarchical ZSM-48 exhibited excellent hexane cracking activity compared to parent ZSM-48, which can be attributed to better diffusion as a result of the created mesoporosity. Moreover, the post-synthesis treatment allowed for manipulation of the distribution of active sites. Consequently, better stability and higher propylene selectivity were accomplished. The spent catalyst was regenerated by removing the deposited coke from the pores, and the regenerated catalyst was characterized again to investigate the recyclability of the hierarchical structure achieved. Parent ZSM-48 showed the same textural and acidic properties after regeneration, while the structure of the post-treated sample suffered from serious defects. The defects severely decreased the number of active sites as measured by pyridine Fourier transform infrared spectroscopy and caused major structural collapse as observed by scanning electron microscopy and transmission electron microscopy.

1. INTRODUCTION

The demand of light olefins, especially ethylene and propylene, is growing fast because they represent the raw materials for different petrochemical industries.[1−3] Naphtha cracking is the major process, which supplies the requested amounts of these olefins.[4,5] The catalytic cracking of naphtha is a more promising technology to boost the selectivity toward desired products.[6,7] Zeolites are representing the most favorable catalyst in such a type of reaction as a result of their cost-effectiveness and good cracking performance.[8,9] One-dimensional zeolites, which have rarely been used because of their quick deactivation problem are given higher selectivity toward light olefins compared to three-dimensional zeolites.[6,10] The main cause of deactivation in one-dimensional zeolites is due to diffusion limitation, which gives a chance for severe naphtha cracking and, consequently, deposition of coke inside the pores.[11,12] Therefore, many groups applied post-synthesis desilication and dealumination to enhance the diffusion and create more mesoporosity and developed what is called as hierarchical zeolites.[13−19]

ZSM-48 (MRE) is one-dimensional zeolite with a 10-membered ring pore system with a pore opening of 5.3 × 5.6 Å. It is known as a high-silica zeolite with a disordered structural framework of ferrierite sheets connected together.[20,21] ZSM-48 showed interesting catalytic performance in different reactions, such as hexane hydrocracking,[21] hexane cracking,[6] and methanol to hydrocarbons.[22]

Fluid catalytic cracking (FCC) is the second most major unit of propylene production.[23] Catalyst bed fluidization is one of the successful process design solutions to overcome the quick catalyst deactivation.[24,25] In this process, the catalyst is continuously regenerated to preserve a certain level of performance.[25] The regenerator part is simply a furnace used to burn the formed coke over the catalyst.[26] Therefore, it is highly important to study the effect of the regeneration process on the properties of the catalyst to ensure the same performance when the catalyst is reused again.

The main scope of this work is to investigate the changes in physiochemical properties of the regenerated post-synthesis-treated ZSM-48 catalyst after they were evaluated in hexane cracking. Hexane is commonly used as a model compound for light naphtha.[27,28] This work will be helpful to judge and assess the stability and durability of the post-synthesis-treated route in preparing hierarchical zeolites, especially because the structure of these hierarchical zeolites is suffering from serious defects. The durability and preservation of zeolite properties are highly required for the catalyst, which will be used in FCC or any process because the calculations of material balance of separation units will be based on product selectivity.

Received: September 17, 2017
Revised: October 31, 2017
Published: October 31, 2017

DOI: 10.1021/acs.energyfuels.7b02796
Energy Fuels XXXX, XXX, XXX−XXX

2. EXPERIMENTAL SECTION

2.1. Synthesis of Parent ZSM-48. A crystalline phase of ZSM-48 was synthesized by dissolving 0.48 g of NaOH in 54 mL of deionized water. A total of 0.08 g of $Al(OH)_3$ was added to the solution as a source of Al. After the solution became homogeneous, 0.91 g of hexamethonium bromide was added as an organic structure-directing agent (OSDA). Later, 9 g of fumed silica was added slowly to the solution as a source of silica. The gel was stirred for 6 h in room temperature before it was transferred to a Teflon-lined stainless-steel autoclave. The final gel composition was $SiO_2/0.0033Al_2O_3/0.08$ $NaO_2/0.0167HMBr/20H_2O$. The polytetrafluoroethylene (PTFE) holder was placed in a conventional oven for 72 h at 190 °C. The Si/Al ratio of the gel was 150. The products were then washed several times with distilled water to normalize the pH to 7.

2.2. Preparation of Hierarchical ZSM-48. Post-synthesis treatments were applied on calcined ZSM-48 crystals, which were obtained in section 2.1. Typically, 1 g of parent ZSM-48 was treated with 30 mL of solution of 0.15 M NaOH at 75 °C for 30 min. The powder was then separated and washed. The sample was named as ZM-0.2. Another hierarchical sample was prepared by expose the alkaline-treated sample to one-step acid treatment by nitric acid. A total of 1 g of alkaline ZSM-48 was added to 30 mL of 2 M HNO_3. The treatment was performed at 75 °C for 20 min. The remaining powder was separated and washed by distilled water several times. The protonated form of the parent and post-treated samples were obtained by ion exchange with 2 M NH_4NO_3 at 80 °C for 30 min. The final calcination was performed at 550 °C for 12 h to obtain the H form of the zeolite.

2.3. Catalytic Performance Evaluation. Catalytic cracking of *n*-hexane was performed in a fixed-bed reactor connected online to Shimadzu GC-2014. Typically, 100 mg of the catalyst was pelletized in the range of 300−500 nm, loaded in a quartz tube supported over glass wool, and placed inside the furnace. Hexane was fed to the reactor by a syringe pump at a rate of 1.2 mL/h derived by nitrogen as a carrier gas with a rate of 20 mL/h. The weight hourly space velocity (WHSV) was adjusted to 8 h^{-1}. Before starting the reaction, the catalyst was calcined for 30 min at 650 °C in air flow with a rate of 20 mL/h. The reaction was performed at 650 °C.

2.4. Characterization. MiniFlex, a Rigaku diffractometer with Cu Kα radiation, was used to record X-ray diffraction (XRD) patterns of the dried solid powder products. The analysis was performed in the range of 5−50° of 2θ with a scan step of 0.03° and a counting time of 4 s for each step. Field-emission scanning electron microscopy (FE-SEM) was used to study the morphology and chemical composition of the samples (LYRA3 dual beam, TESCAN) equipped with energy-dispersive X-ray spectrometry (EDX, Oxford Instruments) operated at an acceleration voltage of 30 kV. N_2 adsorption−desorption was measured using a Micromeritics ASAP 2020 porosimeter. Prior to measurement, the samples were degassed at 623 K for 12 h to remove any possible adsorbed gases. Thermogravimetric analysis and differential scanning calorimetry (TGA/DSC) experiments were carried out under argon gas using a heating rate of 10 K/min up to 973 K. Pyridine adsorption was followed by infrared (IR) spectroscopy (Nicolet 6700 spectrometer) in transmission mode. Spectra were recorded at 4 cm^{-1} spectral resolution, an undersampling ratio of 4, and a speed of 20 kHz. Samples of fresh catalysts were first pressed into thin wafers and then activated *in situ* in the IR cell under secondary vacuum (10^{-6} mbar) at 773 K. After that, the sample cooled to 423 K and pyridine was introduced to the cell for 30 min.

Solid-state ^{27}Al magic angle spinning nuclear magnetic resonance (MAS NMR) was performed in a Bruker Avance 400 MHz. A 4000 spinning rate was used for the treated samples. Aluminum sulfate was used as a standard for the aluminum peak.

Transmission electron microscopy (TEM) was carried out in a field emission gun FEI F30 electron microscope, equipped with a STEM-HAADF module, an EDAX EDS detector, and a Gatan Tridiem energy filter (EELS/EFTEM) with a charge-coupled device (CCD, 2000 × 2000). Prior to observation, the samples were dispersed in ethanol and a few drops of the suspension were placed onto a carbon-coated copper microgrid.

3. RESULTS AND DISCUSSION

3.1. Changes in ZSM-48 Crystallinity. *3.1.1. Changes in ZSM-48 Crystallinity, Morphology, and Composition as a Result of Post-Synthesis Treatments.* The post-synthesis treatments, which were applied on ZSM-48, resulted in some structural defects, as noted in XRD patterns in Figure 1.

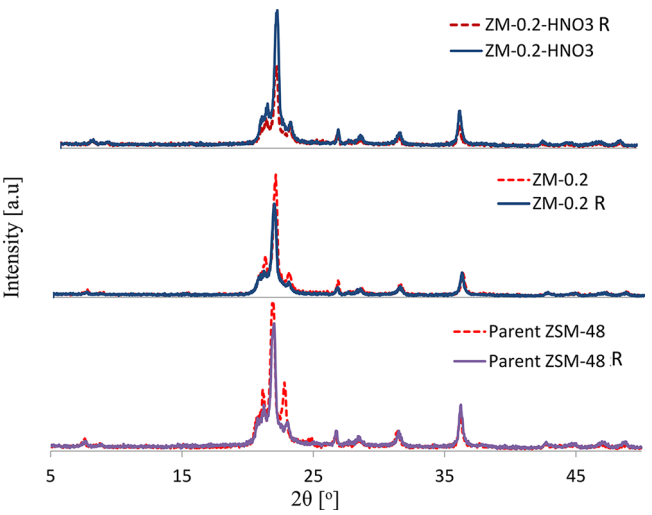

Figure 1. XRD patterns of parent and hierarchical ZSM-48 catalysts before reaction and after regeneration.

Successful extraction of some Si species from the framework of ZSM-48 was achieved as a result of the treatment with 0.2 M NaOH. This Si extraction was confirmed by EDX results, which show that the Si/Al ratio in parent ZSM-48 decreased from 150 to 83 after alkaline treatment, as shown in Table 1. However,

Table 1. Si/Al Ratios and Crystallinities of Fresh and Regenerated ZSM-48 Samples

sample	Si/Al	relative crystallinity
parent ZSM-48	150	100
ZM-0.2	83	76
ZM-0.2-HNO_3	173	94
parent ZSM-48 R		91
ZM-0.2 R		69
ZM-0.2-HNO_3 R		62

excessive Al removal was observed after sequential acid treatment for the desilicated sample. Upon the literature survey, it appears that the desilication treatment of one-dimensional zeolites leads to the removal of some Al from the framework.[14,29] Removed Al does not have the affinity to stay in the alkaline solution; therefore, it favors to be redeposited again on the outer pores of the crystals, as some researchers called realumination.[15,30] The deposition of this amorphous layer of non-framework Al usually causes a reduction in zeolite crystallinity, which explains the reduction in the crystallinity of ZM-0.2 to 76% compared to parent ZSM-48, besides the structural defects caused by desilication. Consequently, to remove extra-framework Al (EFAl) species, the previous alkaline treatment of ZSM-48 was followed by an acid treatment. Effectively, the acid treatment recovered the

DOI: 10.1021/acs.energyfuels.7b02796
Energy Fuels XXXX, XXX, XXX−XXX

reduction in crystallinity of ZM-0.2 because it has again increased to 94% in ZM-0.2-HNO_3, which makes it possible to claim the 6% reduction in the crystallinity to the demetalation defects. In fact, the effect of acid treatment was not limited only to EFAl species but also reached framework Al because the EDX result of ZM-0.2-HNO_3 shows that the Si/Al ratio is 173, which is even higher than the parent sample.

The change in morphology of parent and treated ZSM-48 was examined by a SEM micrograph, as presented in Figure 2.

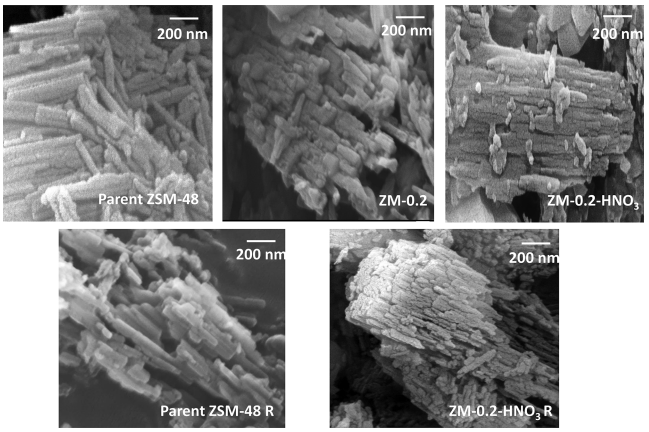

Figure 2. SEM micrographs of parent and hierarchical ZSM-48 catalysts before reaction and after regeneration.

The parent ZSM-48 image shows typical cylindrical crystals of ZSM-48 in an average length of 400−500 nm. After the desilication treatment, sample ZM-0.2 shows more agglomeration, which can be explained by the deposition of amorphous Al in the space between the crystals. However, this agglomeration was not observed in the ZM-0.2-HNO_3 sample, which confirms the previous hypothesis.

The created mesoporosity on treated sample ZM-0.2-HNO_3 was observed clearly on TEM images, as shown in Figure 3. Mainly, intercrystalline mesopores was observed in the range of 10−20 nm.

3.1.2. Changes in Crystallinity as a Result of Catalyst Regeneration. Relative crystallinity was measured after all of the tested samples were calcined to reactivate the catalyst by removing the coke. Crystallinity is an important indication for zeolite structural quality. The decrease in relative crystallinity is usually due to either the presence of the amorphous phase together with the crystalline phase, structural collapse, or both reasons together. The relative crystallinity of parent ZSM-48 was decreased to 91% after the testing and regeneration, which is acceptable as a result of the high temperature used in the reaction, which was 650 °C. The relative crystallinity of the desilicated sample ZM-0.2 was extremely decreased, as discussed before; furthermore, it was subjected to decrease more to reach 69% after coke removal. Surprisingly, after the relative crystallinity of ZM-0.2-HNO_3 was recovered by acid treatment, as discussed previously, it was significantly decreased from 94 to 62% after the reaction and regeneration (Figure 4). Definitely, this decrease is not a good sign for catalyst stability, and major changes in textural and acidic properties are expected.

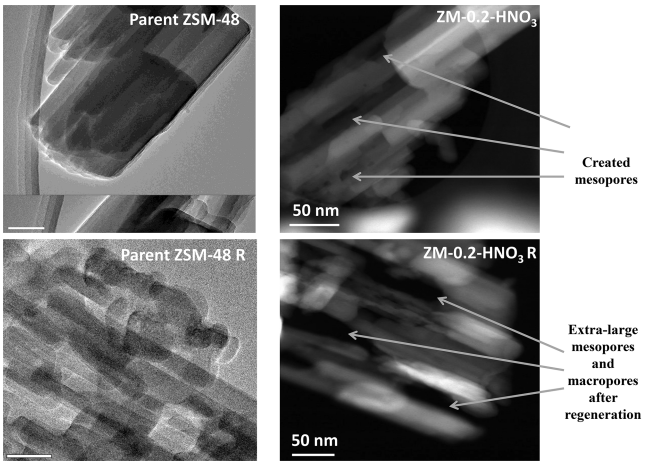

Figure 3. TEM and scanning transmission electron microscopy (STEM) images of parent and hierarchical ZSM-48 before reaction and after regeneration.

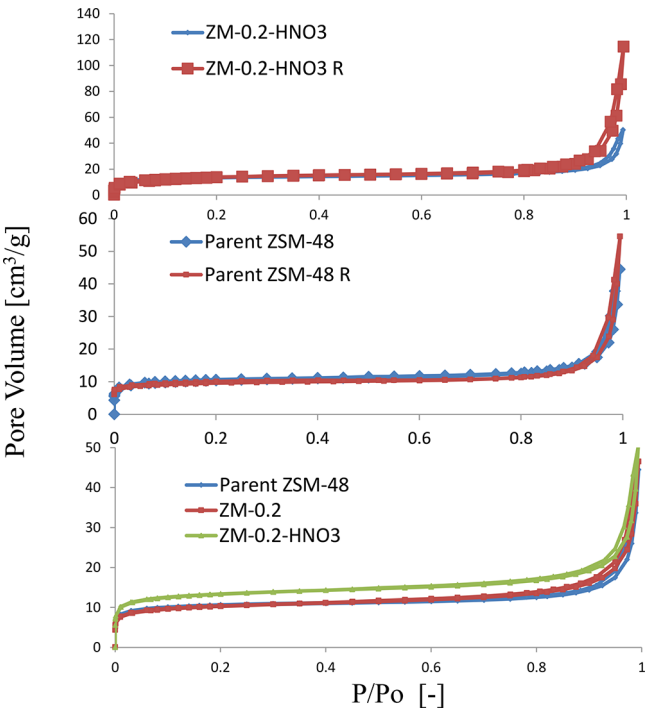

Figure 4. Nitrogen adsorption−desorption isotherms of parent and hierarchical ZSM-48 catalysts before reaction and after regeneration.

3.2. Effects on Physiochemical Properties of ZSM-48.

3.2.1. Changes in Textural Properties as a Result of Post-Synthesis Treatments. Typical post-synthesis demetalation treatments that caused different changes in textural properties depend upon many factors, such as the strength of the zeolite structure, Si/Al ratio, and treatment conditions. In the case of ZSM-48 here, the treatment with 0.2 M NaOH caused an increase in the mesoporosity surface area from 32 to 45 m^2/g as a result of the creation of more mesopores, as presented in Table 2. However, on the other hand, microporosity was decreased from 201 m^2/g in the case of parent ZSM-48 to 191 m^2/g, which can be attributed to the deposition of EFAl species on the pores.

The non-framework Al species were later removed by applying acid treatment, which gave a significant increase in microporosity from 191 m^2/g in ZM-0.2 to 226 m^2/g in ZM-0.2-HNO_3, as presented in Table 2. The amount of

DOI: 10.1021/acs.energyfuels.7b02796
Energy Fuels XXXX, XXX, XXX−XXX

Table 2. Textural Properties of Parent, Treated, and Regenerated ZSM-48 Zeolites

sample	S_{micro} (m^2/g)	S_{meso} (m^2/g)	V_{total} (cm^3/g)	V_{meso} (cm^3/g)
parent ZSM-48	201	32	0.027	0.0015
ZM-0.2	191	45	0.038	0.0092
ZM-0.2-HNO_3	126	48	0.043	0.0127
parent ZSM-48 R	100	31	0.027	0.0015
ZM-0.2-HNO_3 R	125	90	0.057	0.0361

microporosity after the sequential alkaline and acid treatments was more than what was observed in parent ZSM-48. This increment in microporosity gave an indication that the parent sample had some amount of non-framework Al species block some of the pores, which were effectively removed by acid treatment. This assumption was strongly supported by ^{27}Al NMR analysis of parent and treated ZSM-48 samples, as shown in Figure 5. The spectra show that the parent ZSM-48 sample

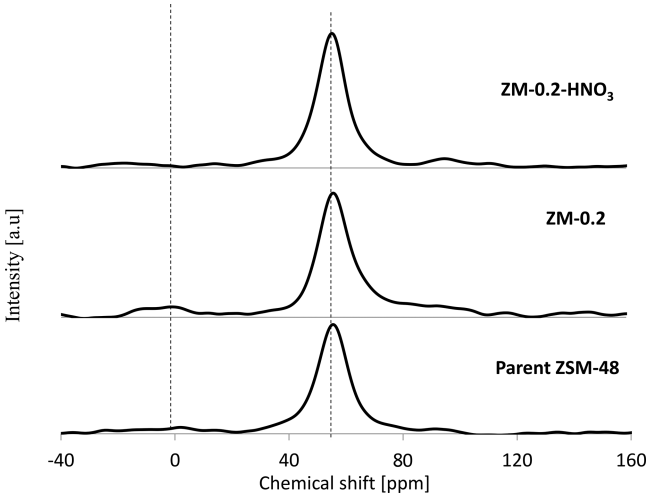

Figure 5. ^{27}Al NMR of parent and hierarchical ZSM-48.

has a small broad peak around 0 ppm, which is attributed to non-framework Al. This peak becomes bigger in the case of ZM-0.2, which is an indication that more non-framework Al species appeared in this sample. After the acid treatment, this peak totally disappeared, as a definite sign of removing non-framework Al species. Therefore, both micro- and mesoporosities were increased by the acid treatment.

The pore size distribution, achieved by applying the Barrett–Joyner–Halenda (BJH) method, is presented in Figure 6. The pore size distribution is showing that ZM-0.2-HNO_3 has the highest mesoporosity compared to other samples and the mesopore size is around 25–50 nm.

3.2.2. Changes in Textural Properties as a Result of Catalyst Regeneration. The spent samples, after catalytic evaluation testing in hexane cracking of ZSM-48, were calcined at 550 °C for 6 h to study the effect of regeneration on textural properties. Parent ZSM-48 showed the same micro- and mesoporosities after regeneration. This observation confirms that the structure of parent ZSM-48 was not affected by coke removal and the porosity was preserved. On the other hand, the hierarchical sample, which was achieved by sequential alkaline and acid treatments of ZM-0.2-HNO_3, exhibited dramatic changes in textural properties. A massive decrease in micro-porosity was noted on ZM-0.2-HNO_3 after regeneration, as a

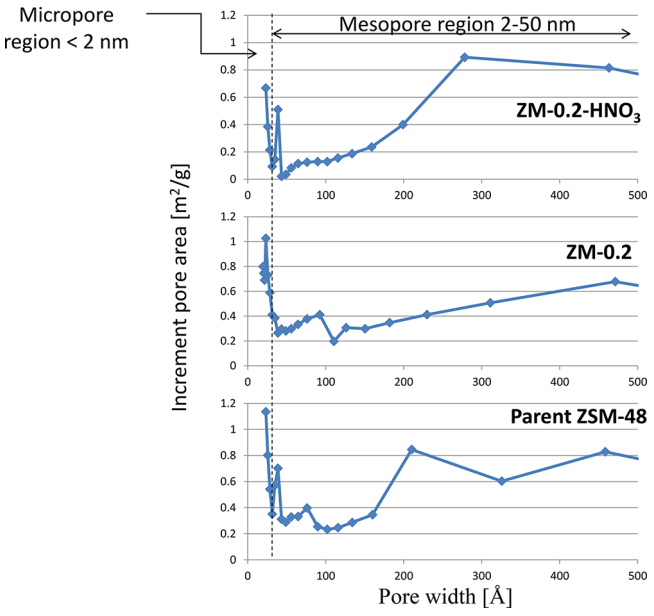

Figure 6. BJH pore size distribution of parent and hierarchical ZSM-48.

quarter of these pores was lost, as shown in Table 2. In the meantime, the mesoporosity was increased from 48 to 90 m^2/g after the calcination and coke removal. These results are in a good agreement with XRD results of crystallinity, which were discussed before. It seems that the majority of microporosity was destroyed and converted to larger pores and the created amorphous silica blocked some of the microporosity.

3.3. Effects on ZSM-48 Acidity. *3.3.1. Changes on Acidity as a Result of Post-Synthesis Treatments.* The defects, which were created on the ZSM-48 structure, caused critical variations in acidity distribution between Brønsted and Lewis active sites, as observed by pyridine Fourier transform infrared spectroscopy (FTIR) analysis (Figure 7). After the desilication treatment, the amount of Lewis acidity was considerably increased from 12.2 to 20.4 mmol/g, as shown in Table 3. The increase in Lewis acidity can be attributed to the formation of

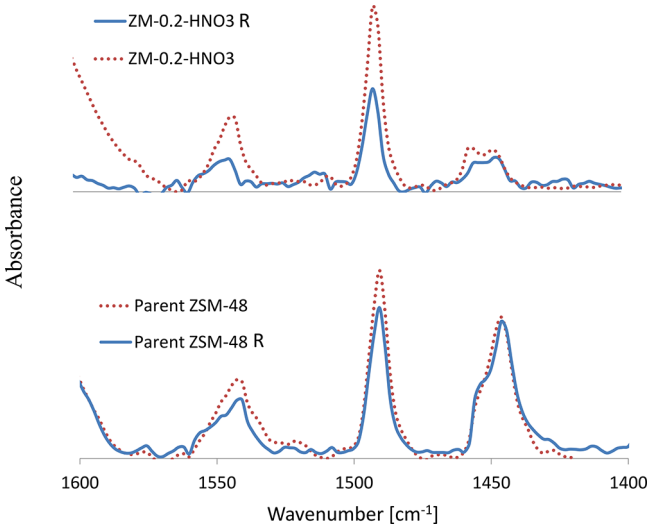

Figure 7. Pyridine FTIR adsorption spectra of parent and hierarchical ZSM-48 before reaction and after regeneration.

DOI: 10.1021/acs.energyfuels.7b02796
Energy Fuels XXXX, XXX, XXX–XXX

Table 3. Acidic Properties and Deposited Coke of Fresh and Regenerated ZSM-48 Zeolites

sample	Brønsted acid sites (mmol/g)	Lewis acid sites (mmol/g)	total acidity (B + L) (mmol/g)	coke (%)
parent ZSM-48	32.7	12.2	44.9	6.9
ZM-0.2	14.3	20.4	34.7	2.4
ZM-0.2-HNO_3	24.9	15.9	40.8	2.1
parent ZSM-48 R	29.7	12.4	42.1	
ZM-0.2 R	14.1	25.7	39.8	
ZM-0.2-HNO_3 R	10.2	9.5	29.7	

more EFAl species, besides the removal of some Si from the ZSM-48 structure. Meanwhile, the Brønsted acidity of the ZM-0.2 sample was remarkably decreased to reach almost half the amount in the parent ZSM-48 sample. This decrease can be explained by the deposition of EFAl species on the active Brønsted sites.

The sequential acid treatment, which followed the alkaline treatment, removed a considerable amount of non-framework Al, which consequently opens access to the blocked Brønsted sites; therefore, Brønsted acidity was increased from 14.3 mmol/g in the case of the ZM-0.2 sample to 24.9 mmol/g in the case of ZM-0.2-HNO_3. In the meantime, the Lewis acidity was decreased from 20.4 to 15.9 mmol/g because of the removal of EFAl species, as confirmed by ^{27}Al NMR results.

3.3.2. Changes in Acidity as a Result of Catalyst Regeneration. The acid active sites were calculated after the spent samples were regenerated, as presented in Table 3. The Lewis active sites did not change after regeneration, while the Brønsted acidity was slightly decreased in the case of the parent ZSM-48 sample, which indicates good structural stability. Interestingly, a considerable decrease in both Lewis and Brønsted acidities was observed on hierarchical sample ZM-0.2-HNO_3 after regeneration. Basically, regeneration was performed to reactivate the catalyst by removing the deposited coke, which was attached to the active sites as a result of excessive cracking. With reference to Brunauer–Emmett–Teller (BET) and XRD results of the ZM-0.2-HNO_3 sample, which showed a large increase in mesoporosity and an extensive decrease in microporosity and crystallinity, it will be possible to conclude that the removal of coke in the regeneration step caused a leaching in framework Si and formed non-framework silicon species, which are catalytically inactive. Unfortunately, this conclusion is showing that the hierarchical structure of ZSM-48 fabricated by the post-synthesis route was very weak compared to the parent ZSM-48 sample because critical transformation of the tetrahedral Si coordination to extra-framework Si species was noted. This extraordinary decrease in both active sites and microporosity is a clear sign for major structural collapse. The stable structure of the parent ZSM-48 sample was capable of maintaining the same textural and acidic properties after regeneration, even though it was loaded by a higher amount of coke at 6.9% compared to 0.8% on ZM-0.2-HNO_3 (Table 3).

3.4. Hexane Cracking over Hierarchical ZSM-48. The catalytic cracking performance of parent ZSM-48 was not exciting because the initial conversion of hexane did not exceed 20%, as shown in Figure 8. This modest performance can be attributed to the entrapping of some products inside the pores and subjected to further cracking, which resulted depositing coke on the pores. This hypothesis was confirmed by the large amount of coke formed on this sample (6.9%), as presented in Table 3. Moreover, the desilicated sample ZM-0.2 showed worse cracking results compared to parent ZSM-48. The initial hexane conversion was ca. 13% and declined to less than 10% after 140 min on stream. These results are in good agreement with diffusion results, which were discussed in section 3.2.1, in which the EFAl species eliminated the diffusion of the reactant and products through the pores.

On the other hand, the sequentially treated sample ZM-0.2-HNO_3 exhibited significant enhancement in the cracking performance compared to the other samples. The initial conversion was 55% and declined to 30% after 140 min time

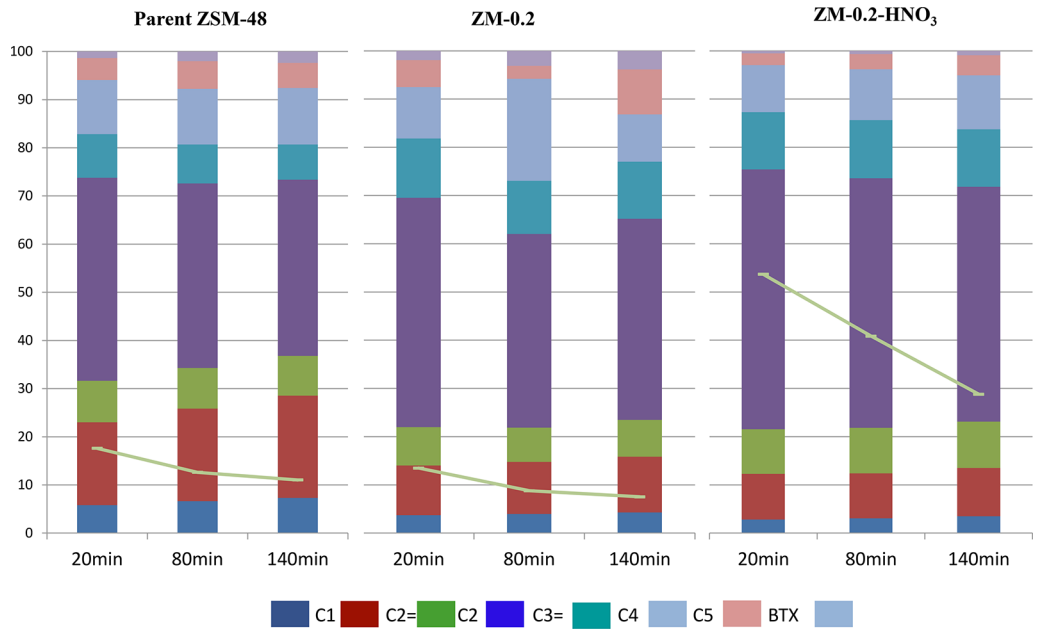

Figure 8. Product selectivity and hexane conversion over parent and hierarchical ZSM-48. Reaction conditions: catalyst weight, 10 mg; WHSV, 8 h^{-1}; and temperature, 650 °C.

DOI: 10.1021/acs.energyfuels.7b02796
Energy Fuels XXXX, XXX, XXX–XXX

on stream (TOS). The hierarchical structure of ZM-0.2-HNO_3 offered better selectivity toward propylene because the initial yield reached 34% compared to only 13% in the case of parent ZSM-48. The observed improvement in catalyst activity can be explained by the existence of more mesoporosity, which facilitated the diffusion. Moreover, the increase in Lewis acidity in ZM-0.2-HNO_3 compared to parent ZSM-48 enhanced the dehydrogenation of paraffins to produce more olefins, as known by secondary reaction.[17] Those two factors together reduced the formation of coke because only 2.4% of coke formed after 140 min. Moreover, the total yield of olefins increased from 18 to 40%, which gives an important advantage to the created hierarchical structure, as shown in Table 4.

Table 4. Product Yield of Parent and Hierarchical ZSM-48

sample	TOS (min)	paraffins	olefins	aromatics
parent ZSM-48	15	12.2	18.4	0.4
	80	9.4	13.4	0.4
	140	7.1	10.4	0.4
ZM-0.2-HNO_3	15	23.0	40.3	0.0
	80	19.3	30.8	0.0
	140	15.1	22.0	0.0

Recently, it is becoming undoubtable that the hierarchical structure of zeolite gives excellent catalytic results compared to the typical microporous structure. However, this work is raising an important point about the stability of this structure. The characterization results showed a dramatic collapse in the microporous structure, which resulted in a serious decrease in active sites, when the hierarchical sample was regenerated. On the other hand, parent ZSM-48 exhibited the same textural and acidic properties after regeneration. Consequently, regenerated parent ZSM-48 is expected to give the same cracking performance as in the first cycle. However, regenerated ZM-0.2-HNO_3 is expected to show worse catalytic performance in the second cycle compared to the first cycle. Therefore, this stability issue will be a large drawback in applying the hierarchical zeolites fabricated by the post-synthesis route in real industry.

4. CONCLUSION

Despite numerous works on post-synthesis alkaline and acid treatments to design hierarchical zeolites, there was no research work emphasized the stability of the achieved hierarchical structure. In this work, mesoporous ZSM-48 achieved by sequential alkaline and acid treatments showed excellent cracking performance compared to the parent sample. Meanwhile, this sample exhibited poor stability after regeneration because significant changes were observed in textural and acidic properties. The structural failure of the hierarchical catalyst with a one-dimensional pore system was even observed without applying the typical conditions of a FCC unit, which required circulating the catalyst between the reactor and regenerator at a high pressure. This circulation even required strong mechanical properties for the catalyst to handle the severe environment of high pressure and temperature. Therefore, to consider hierarchical zeolites, fabricated by the post-synthesis route for real industrial applications, effective development in structural stability should be achieved.

AUTHOR INFORMATION

Corresponding Author

*E-mail: omuraza@kfupm.edu.sa.

ORCID

Oki Muraza: 0000-0002-8348-8085

Victor Sebastian: 0000-0002-6873-5244

Notes

The authors declare no competing financial interest.

ACKNOWLEDGMENTS

The authors thank the funding provided by Saudi Aramco for supporting this work through Project Contract 6600011900 as part of the oil upgrading theme at King Fahd University of Petroleum and Minerals.

REFERENCES

(1) Corma, A.; Melo, F. V.; Sauvanaud, L.; Ortega, F. *Catal. Today* **2005**, *107−108*, 699−706.

(2) Bortnovsky, O.; Sazama, P.; Wichterlova, B. *Appl. Catal., A* **2005**, *287*, 203−213.

(3) Mei, C.; Wen, P.; Liu, Z.; Liu, H.; Wang, Y.; Yang, W.; Xie, Z.; Hua, W.; Gao, Z. *J. Catal.* **2008**, *258*, 243−249.

(4) Mochizuki, H.; Yokoi, T.; Imai, H.; Namba, S.; Kondo, J. N.; Tatsumi, T. *Appl. Catal., A* **2012**, *449*, 188−197.

(5) Konno, H.; Tago, T.; Nakasaka, Y.; Ohnaka, R.; Nishimura, J.-i.; Masuda, T. *Microporous Mesoporous Mater.* **2013**, *175*, 25−33.

(6) Zhang, Y.-F.; Liu, X.-L.; Sun, L.-Y.; Xu, Q.-H.; Wang, X.-J.; Gong, Y.-J. *Fuel Process. Technol.* **2016**, *153*, 163−172.

(7) Yamaguchi, A.; Jin, D.; Ikeda, T.; Sato, K.; Hiyoshi, N.; Hanaoka, T.; Mizukami, F.; Shirai, M. *Fuel Process. Technol.* **2014**, *126*, 343−349.

(8) Inagaki, S.; Takechi, K.; Kubota, Y. *Chem. Commun.* **2010**, *46*, 2662−2664.

(9) Kubota, Y.; Inagaki, S.; Takechi, K. *Catal. Today* **2014**, *226*, 109−116.

(10) Muraza, O.; Bakare, I. A.; Tago, T.; Konno, H.; Taniguchi, T.; Al-Amer, A. M.; Yamani, Z. H.; Nakasaka, Y.; Masuda, T. *Fuel* **2014**, *135*, 105−111.

(11) Guisnet, M.; Costa, L.; Ribeiro, F. R. *J. Mol. Catal. A: Chem.* **2009**, *305*, 69−83.

(12) Yoo, K.; Smirniotis, P. G. *Appl. Catal., A* **2003**, *246*, 243−251.

(13) Hartmann, M.; Machoke, A. G.; Schwieger, W. *Chem. Soc. Rev.* **2016**, *45*, 3313−3330.

(14) Ahmed, M. H. M.; Muraza, O.; Al Amer, A. M.; Sugiura, Y.; Nishiyama, N. *Microporous Mesoporous Mater.* **2015**, *207*, 9−16.

(15) Ahmed, M. H. M.; Muraza, O.; Al-Amer, A. M.; Miyake, K.; Nishiyama, N. *Appl. Catal., A* **2015**, *497*, 127−134.

(16) Ahmed, M. H. M.; Muraza, O.; Yoshioka, M.; Yokoi, T. *Microporous Mesoporous Mater.* **2017**, *241*, 79−88.

(17) Ahmed, M. H. M.; Muraza, O.; Jamil, A. K.; Shafei, E. N.; Yamani, Z. H.; Choi, K.-H. *Energy Fuels* **2017**, *31*, 5482−5490.

(18) Pérez-Ramírez, J.; Christensen, C. H.; Egeblad, K.; Christensen, C. H.; Groen, J. C. *Chem. Soc. Rev.* **2008**, *37*, 2530−2542.

(19) Bonilla, A.; Baudouin, D.; Pérez-Ramírez, J. *J. Catal.* **2009**, *265*, 170−180.

(20) Lobo, R. F.; Van Koningsveld, H. *J. Am. Chem. Soc.* **2002**, *124*, 13222−13230.

(21) Bhattacharya, D.; Chatterjee, M.; Sivasanker, S. *React. Kinet. Catal. Lett.* **1997**, *60*, 395−403.

(22) Teketel, S.; Skistad, W.; Benard, S.; Olsbye, U.; Lillerud, K. P.; Beato, P.; Svelle, S. *ACS Catal.* **2012**, *2*, 26−37.

(23) Wang, G.; Xu, C.; Gao, J. *Fuel Process. Technol.* **2008**, *89*, 864−873.

(24) Corma, A.; Melo, F.; Sauvanaud, L.; Ortega, F. J. *Appl. Catal., A* **2004**, *265*, 195−206.

(25) Bryden, K.; Singh, U.; Berg, M.; Brandt, S.; Schiller, R.; Cheng, W.-C. Fluid Catalytic Cracking (FCC): Catalysts and Additives. *Kirk-*

DOI: 10.1021/acs.energyfuels.7b02796
Energy Fuels XXXX, XXX, XXX−XXX

443 *Othmer Encyclopedia of Chemical Technology*; John Wiley & Sons, Inc.:
444 Hoboken, NJ, 2015; pp 1−37, DOI: 10.1002/0471238961.fluid-
445 nee.a01.pub2.
446 (26) Sadeghbeigi, R. *Fluid Catalytic Cracking Handbook: An Expert*
447 *Guide to the Practical Operation, Design, and Optimization of FCC Units*,
448 3rd ed.; Butterworth-Heinemann: Oxford, U.K., 2012.
449 (27) Van Geem, K. M.; Reyniers, M. F.; Marin, G. B.; Song, J.;
450 Green, W. H.; Matheu, D. M. *AIChE J.* **2006**, *52*, 718−730.
451 (28) Rownaghi, A. A.; Rezaei, F.; Hedlund, J. *Chem. Eng. J.* **2012**, *191*,
452 528−533.
453 (29) Verboekend, D.; Chabaneix, A. M.; Thomas, K.; Gilson, J. P.;
454 Pérez-Ramírez, J. *CrystEngComm* **2011**, *13*, 3408−3416.
455 (30) Ahmed, M. H.; Muraza, O.; Yoshioka, M.; Yokoi, T. *Microporous*
456 *Mesoporous Mater.* **2017**, *241*, 79−88.

DOI: 10.1021/acs.energyfuels.7b02796
Energy Fuels XXXX, XXX, XXX−XXX